

# **The Influence of the Solar Cycle and QBO on the Late Winter Stratospheric Polar Vortex**

**Charles D. Camp\* and Ka-Kit Tung**

Department of Applied Mathematics

University of Washington, Seattle

---

\**Corresponding author address:* Charles D. Camp, University of Washington, Box 352420, Seattle, WA 98195.  
E-mail: [cdcamp@amath.washington.edu](mailto:cdcamp@amath.washington.edu)

## Abstract

Using more than four decades of NCEP/NCAR Reanalysis data, we show that in late winter (February) in the Northern Hemisphere, the 11-year solar cycle (SC) provides a perturbation to the polar stratospheric vortex comparable to that of the Quasi-Biennial Oscillation (QBO). In a four-group (SC max vs. min and east- vs. west-phase QBO) discriminant analysis, the state of the westerly phase QBO during SC min emerges as a distinct least-perturbed (and coldest) state of the stratospheric polar vortex. Relative to this least-perturbed state, SC max and easterly QBO each provides perturbation and warming. When only years during QBO westerly phase are considered, the polar temperature is positively correlated with the SC, with a statistically significant zonal mean warming of approximately 4 °C in the 10-50 hPa layer. This magnitude of warming in winter is too large to be explainable by UV radiation alone. The evidence seems to suggest that the polar warming in NH late winter during SC max is due to the occurrence of Sudden Stratospheric Warmings during QBO westerly phase, which normally do not have Sudden Warmings. Our observational result gives the first suggestion of a powerful dynamical amplifier for solar-cycle radiative heating in the polar stratosphere.

The Holton-Tan effect, whereby the polar vortex is warmer in QBO easterly phase than in QBO westerly phase, is also seen in our data and was found to be statistically significant prior to the last solar cycle. However, it found to not be robust when data from the latest solar cycle is included in the analysis.

# 1. Introduction

The polar stratosphere in the Northern Hemisphere has large interannual variability during winter. The lower stratosphere is much warmer than can be explained from radiative considerations alone, especially during the polar night. The difference in temperature between the observed polar temperature and its radiative equilibrium value is now understood to be provided by the dynamical heating by the planetary waves forced near the surface and propagated upward into the lower stratosphere, where they sometimes break and as a consequence deposit their momentum and heat energy. The most spectacular of these breaking events occur in Stratospheric Sudden Warmings (SSW), when, in the course of one week, the temperature of the polar stratosphere can increase by several tens of degrees. It is well known that the easterly phase of the QBO (eQBO) preconditions the polar stratosphere for mid- and late-winter SSWs (McIntyre 1982; Butchart et al. 1982; Smith 1989; Tung and Lindzen 1979a,b; Tung 1979). Dunkerton et al. (1988) found that none of the observed SSWs (up to 1987) had occurred while the QBO was in a deep westerly phase. While the polar vortex during westerly years of the QBO tends to be less perturbed and generally less prone to SSW occurrences, there are nevertheless exceptional years when SSWs do occur (Naito and Hirota 1997, hereafter denoted NH97); these occur during solar-cycle (SC) max. Labitzke (1987) suggested that during westerly QBO years (wQBO), the polar stratosphere is positively correlated with the solar cycle, being warmer during SC max than during SC min. Later, Labitzke and van Loon (1988) further suggested that during eQBO years, the relationship is reversed. That is, during the years when the equatorial QBO is in its easterly phase, the polar stratosphere cools during SC max. The modeling work of Gray et al. (2004) appears to offer some support to this puzzling result, possibly caused by changes in the timing of SSWs; however, as they point out, this part of their result is not statistically significant.

The existence of an 11-year solar-cycle response in the atmosphere has recently been established statistically in Coughlin and Tung (2004a) for the stratosphere and Coughlin and Tung (2004b) in the troposphere, among others (Haigh 2003; Gleisner and Thejll 2003), without regard to the phase of the QBO and without separating into seasons. To help shed some light on possible mechanistic explanations of the SC response, we focus in this paper on the winter season, which is the time of the maximum response, and consider separately the two QBO phases. The method we use in this study is discriminant analysis.

## **2. Methodology**

Linear discriminant analysis (LDA) is a long-standing statistical technique used for the classification of multivariate data into predefined groups (Wilks 1995; Ripley 1996). Schneider and Held (2001) have demonstrated its usefulness for identifying spatial patterns associated with interdecadal variations of surface temperatures. In this study, we apply the technique to identify the spatial patterns that best distinguish the behavior of the stratosphere during the westerly and easterly phases of the equatorial QBO and during SC max and min. LDA focuses on coherent spatial variability as opposed to total variance at each individual grid point. As such, it can often isolate large-scale spatial variability with greater statistical significance than studies using correlations of individual time series. On the other hand, the method may not find statistically significant differences amongst groups if the dominant spatial differences between the groups are not consistent in time.

For a set of multivariate observations, LDA seeks a linear combination of variables, aka canonical variates (CV), for which the separation among pre-defined groups is maximized. A measure of separability can be defined by the ratio of among-group variance to within-group variance, denoted

$\mathcal{R}$ . The first CV maximizes this ratio; higher order CVs also maximize this ratio subject to the constraint of being uncorrelated with all lower order discriminants. Associated with each canonical variate is a discriminating pattern defined as the regression of the data onto the canonical variate. Alternatively, we can consider the patterns to be the spatial structures which best distinguish the observations of each group, while the associated CVs are the time series constructed by projecting the observations onto the patterns. A more detailed discussion of the technique can be found in the appendices of this paper and in Schneider and Held (2001).

It is important to note that the apparent separation, as measured by  $\mathcal{R}$ , is not a robust feature of the analysis. It is biased to large values and in particular is dependent upon the choice of truncation parameter used to reduce the degrees of freedom in the dataset prior to performing the LDA; see Appendix B for more details on this parameter. As such, it should not be used directly to test the statistical significance of our results. Therefore, to test the statistical robustness of each analysis, we perform a bootstrap Monte Carlo tests using 3000 synthetic datasets constructed by resampling with replacement our set of observations while preserving the group structure and truncation parameter of the original analysis. In other words, we randomly choose observations from the original dataset and assign them to a group regardless of their original physical state while preserving the number of observations in each group. For an example, we might need nine randomly chosen years to put into the SCmin-eQBO category. One year randomly picked could be 1990, which originally was a SCmax-eQBO year. “With replacement” means that the next time we pick a year, all the years, including 1990, are again available to be picked. This assures that each random choice is drawn from the same distribution. An LDA is then performed on each synthetic dataset using the same truncation parameter as that used in the original (observed) LDA to create a distribution of variance ratios. The percentile of the observed variance ratio within the distribution

of synthesized variance ratios denotes the statistical significance of that observed ratio; *i.e.*, the percentile subtracted from 100 is the percentage of a random realizations that have a separation equal to or greater than the observed separation.

### 3. Datasets

We use data from the NCEP/NCAR Reanalysis from post Internal Geophysical Year to present, specifically from the late winter of 1958/1959 to the late winter of 2004/2005. We consider the mean temperature in the 10-50 hPa layer, as represented by difference between the 10 and 50 hPa geopotential height surfaces. We use monthly mean data on a  $2.5^\circ \times 2.5^\circ$  latitude-longitude grid restricted to latitudes north of  $30^\circ\text{N}$  excluding the pole. Separate analyses are carried out for individual months and for certain 2 and 3 month averages during the northern winter. The resulting annual datasets are centered by subtracting the mean height difference at each grid point from the corresponding time series. Both the full two-dimensional fields and the corresponding zonally averaged fields are studied. The 2D fields are scaled at each grid point by the square root of the cosine of the latitude to account for the change in the area represented by each grid point.

Observations are assigned to one of four groups: SCmax-wQBO, SCmin-wQBO, SCmax-eQBO, SCmin-eQBO, based on the phases of the indices used in each analysis. For a solar-cycle index, we use the monthly means of the observed daily noon 10.7cm Solar Radio Flux from Ottawa/Penticton for 1949 - 2005. SC-max(min) months are those with fluxes greater(less) than 140(125) solar-flux units (s.f.u.); the mean flux was 132.5 s.f.u. For the equatorial QBO index, we use the monthly mean 30 hPa zonal wind at the equator from the NCEP/NCAR Reanalysis for 1956 - 2005; westerly(easterly)-phase months are those with wind speeds greater(less) than 2.0(-2.0) m/s.

We have found that the correlation of the mean temperature in the 10-50 hPa layer with the solar cycle is different in early winter (centered in November, but can include October and December) from the correlation found in late winter (centered in February, but can include January and March). Therefore, the selection of months in late winter for this study is important. Early winter results will be presented separately in another paper. Because of the large variability in the Northern Hemisphere polar vortex during winter, multiple-month averaging is needed to achieve statistically confident results. Three-month averaging is usually best, but we have attempted to better pinpoint the time by using one- and two-month averages. In general, early winter results can be significant if the chosen period does not include much influence from SSWs which can occur as early as December in some years. Late winter results are similar as long as the averaging period includes February.

## 4. Four Group Analysis

We attempt to discriminate the behavior of the northern hemisphere stratosphere during these years amongst these four groups using the method of Linear Discriminant Analysis (LDA). Figure 1a shows the February-March average of the years used in the analysis, denoted  $\mu(\mathbf{x})$ . This mean state shows a moderately cold polar vortex displaced toward western Europe by a warm wave-one planetary wave.

For a four group analysis there exist three discriminants, consisting of the spatial patterns which best distinguish each group from the other groups and of an associated time series or canonical variate (CV) constructed by projecting the data onto each of the patterns. The CVs are denoted by  $C_1(t)$ ,  $C_2(t)$  and  $C_3(t)$ , while the associated patterns are denoted  $P_1(\mathbf{x})$ ,  $P_2(\mathbf{x})$  and  $P_3(\mathbf{x})$ , respectively. This calculation is done with truncation  $r = 15$  in an EOF expansion. The technical

details on how to choose a truncation level are discussed in the Appendix B. Briefly, since the LDA method attempts to maximize the ratio of between-group variance to within-group variance,  $\mathcal{R}$ , it requires that enough EOFs are kept that help maximize the between-group variance, but not so many are retained that one is in effect fitting smaller-spatial-scale noise to minimize the within-group variance in the denominator of  $\mathcal{R}$ . Figure 1b is a scatter plot of the projection of the years onto the first two discriminant patterns, *i.e.*,  $C_2(t)$  vs.  $C_1(t)$ . It is seen that  $C_1$ , shown as the horizontal axis, primarily isolates the SCmin-wQBO state from the other three states; the separability measure for  $C_1$ ,  $\mathcal{R}_1$ , is approximately 2. The 2nd and 3rd discriminants (not shown) distinguish amongst the other three states, with  $\mathcal{R}_2 \approx 0.5$  and  $\mathcal{R}_3 \approx 0.4$ ; these values are rather small implying that the three perturbed states are not well separated by this analysis. Figure 1c shows the spatial pattern of the first discriminant,  $P_1(\mathbf{x})$ , with warming (cooling) of the polar vortex when  $C_1$  is positive (negative). Furthermore, the the vortex is displaced further off the pole for positive  $C_1$ . Figure 1d shows  $C_1(t)$  as a function of year and shows that negative values of  $C_1$  nicely isolate the SCmin-wQBO years as being colder and less perturbed when compared to the other three groups. It does not appear to distinguish SC-max perturbations from eQBO perturbations, but shows that these two perturbations are comparable in magnitude. Hence the four-group analysis is not statistically significant; yet Figure 1d clearly shows that the SCmin-wQBO group is distinct from the other groups. Representative examples of the unperturbed and perturbed vortex are shown in Figure 2. These are the sum of the mean state and the projection onto the 1st discriminant pattern,  $P_1(\mathbf{x})$ , for individual observations;  $\mu(\mathbf{x}) + C_1(t^*) \cdot P_1(\mathbf{x})$ . A observation from the (SCmin-wQBO) group,  $t^* = 1988$ , depicts the unperturbed vortex (Figure 2a), while an observation from the (SCmax-wQBO) group,  $t^* = 1978$ , depicts the perturbed vortex (Figure 2b). The perturbation associated with  $P_1(\mathbf{x})$  (with positive  $C_1(t)$ ) greatly warms and weakens the polar

vortex. It should be noted that these figures do not capture the full variability of the polar vortex, only that portion which projects onto  $P_1(\mathbf{x})$ . Furthermore,  $P_1(\mathbf{x})$  does not distinguish between perturbations of the polar vortex during SC max from those during the easterly QBO. Therefore, we will perform a series of two-group LDAs to isolate SC effects from QBO effects.

## 5. Solar Cycle Discriminants

To isolate the solar-cycle effect, we perform two-group analyses discriminating SC max from SC min for various sets of years based on the phases of the QBO. This is suggested by the result in Figure 1b, which shows that the SC-max years are separated from the SC-min years during the westerly phase of the QBO, while the separation during the easterly phase is much smaller. Furthermore, since the leading discriminant pattern has a strong zonal mean structure, we analyze the zonally-averaged field. This analysis is simpler to depict and proves to be more statistically significant than the full 2D analysis. We use the same two-month temporal average (February-March) as that used in the four-group LDA done above. The results for other late winter time periods, *e.g.*, January-February, are qualitatively similar but do not prove to be as statistically significant.

The first analysis, shown in Figure 3, discriminates between SC max and SC min for all years, regardless of the phase of the QBO. With only two groups, there is only one discriminant, consisting of the spatial pattern which best distinguishes SC-max years from SC-min years and of the associated canonical variate time series. The analysis is done with a  $r = 14$  truncation. The first discriminant pattern,  $P_1(\mathbf{x})$ , (Figure 3a) displays warming at the pole balanced by cooling in the midlatitudes when  $C_1(t)$  is positive. Figure 3b displays  $C_1(t)$  as a function of years. It shows that SC-max years have predominately positive  $C_1$  values and are reasonably separated,  $\mathcal{R} \approx 2$ ,

from most of the SC-min years, *i.e.*, when  $C_1$  is either negative or near zero. The difference of the mean of  $C_1$  during high solar flux years from the mean during low solar-flux years corresponds to a zonal-mean warming of the pole of approximately 2.5 °C. This can be more readily seen in Figure 3c which gives an alternate presentation of the information already contained in Figures 3a and b. It shows the sum of the spatial pattern,  $P_1(\mathbf{x})$ , and the overall mean (shown in black) where the amplitude of  $P_1(\mathbf{x})$  is determined from the mean of  $C_1$  within each group of years. The SC-max years are in red and the SC-min years are in blue. Shaded regions denoted the one-standard-deviation projections within each group. Figure 3c shows that the SC-max years, when projected onto this coherent spatial pattern, are separated from the SC-min years but with some overlap. However, the Monte Carlo test, Figure 3d, shows that the observed variance ratio is not significant; only achieving a 74% confidence level. Random assignation of observations to each group can provide the observed degree of separation approximately 26% of the time.

### 5a. Westerly QBO years

Another two-group LDA is performed discriminating SC max from SC min, but using only years during the westerly phase of the equatorial QBO (see Figure 4). A  $r = 5$  truncation is used. As in the previous analysis (all QBO years), the resulting pattern shows a warming of the pole and a cooling of the midlatitudes during SC max, Figure 4a. This pattern is generally consistent with the warming and cooling structure resulting from the deposition of easterly momentum in the high-latitude stratosphere (Garcia 1987) and, in particular, with the predicted pattern during a SSW (Matsuno 1971). Compared to the all-QBO-years analysis, the wQBO analysis has a much larger separation,  $\mathcal{R} \approx 6$ , with a clean separation between the positive  $C_1$  values of the SCmax-wQBO group and the mostly negative values of the SCmin-wQBO group; see Figure 4b. This corresponds

to a mean warming of the pole of approximately 3.7 °C. The Monte Carlo test shows that the separation is significant at the 99% confidence level. This is the key positive result of this study.

### **5b. Easterly QBO years**

A third two-group LDA is carried out on the zonally averaged field to distinguish the SC-max years from SC-min years during the eQBO phase, with a  $r = 9$  truncation; see Figure 5. Qualitatively, the pattern of the solar-cycle effect on the polar vortex during easterly QBO years is similar to the pattern during the westerly QBO years albeit with a smaller amplitude and no reversal in the midlatitudes. The discriminant pattern, Figure 5a, displays a warming of the pole of approximately 1.5 °C, as well as a slight warming at the midlatitudes, for positive values of its associated  $C_1(t)$ , Figure 5b. As seen in the westerly phase analysis, high solar-flux years tend to have positive  $C_1$  values denoting a warming of the pole compared to low solar-flux years. However the separation between the groups is not large ( $\mathcal{R} \approx 2$ ) and, unlike the westerly phase result, fails to be statistically significant (34<sup>th</sup> percentile) when the Monte Carlo test is applied. Our result is different than the conclusion of Labitzke and van Loon (1988), who showed that the effect of solar cycle is reversed in the easterly QBO years. However, neither our result nor their result for the eQBO is statistically significant.

### **5c. Summary**

We find a highly statistically significant solar-cycle signal in the polar stratosphere during late winter. It warms the 10-50 hPa layer in the polar stratosphere by about 4 °C during SC-max as compared to SC-min, during the westerly phase of the QBO. Similar effects are found during the

easterly phase of the QBO, as well as over all years regardless of QBO phase, except that these results are not statistically significant.

## 6. QBO Discriminants

Two-group LDA analyses are also performed to distinguish the behavior of the polar vortex between the westerly and easterly phases of the equatorial QBO using various sets of years associated with the solar cycle. A three-month average, January - March, is used for all of the QBO discriminant analyses described in this section.

The results of a two-group LDA discriminating westerly vs. easterly phases of the equatorial QBO, using all years regardless of the phase of the SC are shown in Figure 6; a  $r = 14$  truncation is used. The discriminant pattern, see Figure 6a, shows an oscillation similar to that seen in previous studies (*e.g.*, Holton and Tan 1980, hereafter denoted HT80). When the equatorial QBO is easterly, the polar vortex is warmed by approximately  $2^\circ\text{C}$ . The separability is reasonable,  $\mathcal{R} \approx 3$ . However, the Monte Carlo test shows that it is not significant; only achieving a 77% confidence level.

### 6a. Solar Cycle Min

Given the results of our 4-group analysis, Section 4, and of NH97, our expectation is that the QBO effect may be better isolated during the years of the SC min. Limiting the analysis to SC-min years ( $r = 6$  truncation), we get a discriminant pattern, see Figure 7a, with a similar pattern to that found in the previous (all SC years) analysis albeit with a slightly larger amplitude; warming the pole by approximately  $3^\circ\text{C}$  during eQBO. However, the separability is actually smaller,  $\mathcal{R} \approx 1$ ,

than the all-SC case and is still not significant (24<sup>th</sup> percentile). A more careful examination of the temporal projections in Figure 7b reveals that the poor separation is primarily caused by the years during the latest SC min during the mid 1990s. If the analysis is repeated with only the years from 1958/9 to 1989/90 ( $r = 4$  truncation), a statistically significant separation is achieved ( $\mathcal{R} \approx 7$ , 92% confidence level); see Figure 8. The 1959-1990 result has a warming of the pole associated with the easterly QBO of approximately 4.5 °C.

### **6b.** *Solar Cycle Max*

When we repeat the analysis, limiting it to years during SC max ( $r = 7$  truncation), there is a much smaller warming, approximately 1.5 °C, associated with the eQBO and no significant separation between the wQBO and eQBO data,  $\mathcal{R} < 1$ ; see Figure 9. Unlike the SC-min analysis, Section 6a, this lack of separability is not obviously caused by any one particular solar cycle. It is most likely caused by similarities in the zonal behavior of the SC-max and eQBO perturbations to the unperturbed (SCmin-wQBO) vortex.

### **6c.** *Summary*

These results may imply that the part of the zonal-mean result reported by HT80 may not be robust to the addition of more years. This fact was previously pointed out by NH97. They, however, thought that it was caused by the number of solar maxima vs. solar minima within the period analyzed by HT80. Here we find that, consistent with NH97, there is no Holton-Tan phenomenon in the SC-max years. However, we also find that the highly significant effect found by NH97 for SC-min years is not robust to the addition of another solar cycle.

## 7. Discussion

We observe warming of the polar stratospheric vortex during solar-cycle maxima as compared to solar-cycle minima during late winter. The zonal-mean warming by the solar cycle is statistically significant only when the equatorial QBO is in its westerly phase. This solar-cycle-induced warming during westerly QBO is large, about 4 °C in the zonal mean temperature over the broad layer of 10-50 hPa and appears to be due to dynamical heating arising from SSWs. Although individual SSWs warm the pole by more than 4 °C, their typical duration is approximately one week and therefore a smaller average warming is expected from the multi-month averages used here. The energy for SSWs originates from the denser troposphere; therefore, a modulation of the frequency of SSW occurrence can provide a powerful dynamical amplifier for radiative effect of the solar cycle. Solar-cycle-max conditions appear to precondition the lower stratosphere for SSWs in a similar way as the easterly phase of the QBO preconditions it for SSWs. Thus, we find, as first pointed out by NH97 that the exceptional years when SSWs occur in the westerly phase of the QBO are years of SC max. Our result put this on firmer statistical ground. How the SC max preconditions the stratosphere for SSWs will be studied in a separate paper, which examines its effect on the stratosphere during early winter. In the paper, we have isolated the rather large amplitude of the solar-cycle effect on the polar temperature during February. Since this time is during polar night, it is unlikely to be a radiative effect. While SC max apparently also increases the occurrence of SSW during the easterly phase of the QBO, this effect is not significant probably because easterly phase of the QBO already perturbs the polar stratosphere sufficiently by itself. We are unable to distinguish between SC-max-induced and eQBO-induced perturbations in the zonal-mean analysis. Zonal-wavenumber discriminants will be examined in a separate paper.

We also observe similar warming of polar vortex during the easterly phase of the equatorial

QBO as compared to the westerly phase. The zonal-mean warming induced by the QBO is significant only during solar-cycle minima and only if the data from the latest SC min is excluded from the analysis. The observed warming is about 3 °C in the zonal-mean temperature for the 10-50 hPa layer. Once again, the lack of significance during solar cycle maxima is due, at least in part, to a conflation of SC-max and eQBO perturbations to the unperturbed (SCmin-eQBO) vortex. However, there seems to be a further lack of robustness for the QBO effect caused by changes in the response during the latest solar cycle.

**Acknowledgement** We would like to thank Tapio Schneider for his contribution in useful discussions regarding discriminant analysis and statistical testing. The research was supported by the National Science Foundation under grant ATM-3 32364.

## Appendix A

### Discriminant Analysis

For a set of multivariate observations,  $\mathbf{X}$ , linear discriminant analysis (LDA) seeks a linear combination,  $\mathbf{X}\mathbf{u}$ , for which the separation among pre-defined groups is maximized. The separation can be defined as the ratio of among-group variance to either within-group or total variance. Suppose that we have a centered dataset,  $\mathbf{X}$  ( $n \times p$ ), consisting of  $n$  observations of  $p$  variables,  $\mathbf{x}_i$  ( $1 \times p$ ). Centering is performed by removing the mean observations from the original data. Furthermore, suppose that we can partition the observations into  $g$  groups,  $G_j$  ( $j = 1, \dots, g$ ), with  $n_j$  observations in each group. Let  $\boldsymbol{\mu}_j$  ( $1 \times p$ ) denote the mean of the observations in  $G_j$  and  $[i]$  denote the group of observation  $\mathbf{x}_i$ . We can define the group matrix  $G$  ( $n \times g$ ) =  $[g_{ij}]$ , where

$g_{ij} = 1$  if  $j = [i]$  and equals 0 otherwise. Note that  $\mathbf{G}^T \mathbf{G} = \text{diag}(n_j)$ . Let

$$\mathbf{M}(g \times p) = (\mathbf{G}^T \mathbf{G})^{-1} \mathbf{G}^T \mathbf{X} = [\boldsymbol{\mu}^T]$$

be the matrix of group means. Then the within-group-covariance matrix can be defined as

$$\boldsymbol{\Sigma}_w(p \times p) = \frac{1}{n-g} (\mathbf{X} - \mathbf{GM})^T (\mathbf{X} - \mathbf{GM}),$$

the among-group-covariance matrix as

$$\begin{aligned} \boldsymbol{\Sigma}_a(p \times p) &= \frac{g}{n(g-1)} (\mathbf{GM})^T (\mathbf{GM}) \\ &= \frac{g}{n(g-1)} \mathbf{X}^T \mathbf{G} (\mathbf{G}^T \mathbf{G})^{-1} \mathbf{G}^T \mathbf{X} \end{aligned}$$

and the total-covariance matrix as

$$\boldsymbol{\Sigma}_t(p \times p) = \frac{1}{n-1} \left( (n-g) \boldsymbol{\Sigma}_w + \frac{g}{n(g-1)} \boldsymbol{\Sigma}_a \right).$$

A separability measure for any linear combination  $\mathbf{X}\mathbf{u}$  can then be defined by  $\gamma = (\mathbf{u}^T \boldsymbol{\Sigma}_t \mathbf{u})^{-1} (\mathbf{u}^T \boldsymbol{\Sigma}_a \mathbf{u})$ .

The canonical variates,  $\mathbf{c}_k = \mathbf{X}\mathbf{u}_k$  ( $k = 1, \dots, g-1$ ), are the linear combinations which optimize  $\gamma$ , which implies that  $\mathbf{u}_k$  must satisfy  $\partial\gamma/\partial\mathbf{u} = 2 (\mathbf{u}^T \boldsymbol{\Sigma}_t \mathbf{u})^{-1} \boldsymbol{\Sigma}_a \mathbf{u} - 2 (\mathbf{u}^T \boldsymbol{\Sigma}_t \mathbf{u})^{-2} (\mathbf{u}^T \boldsymbol{\Sigma}_a \mathbf{u}) \boldsymbol{\Sigma}_t \mathbf{u} = 0$ . Therefore, the  $\mathbf{u}_k$  must satisfy  $\boldsymbol{\Sigma}_t^{-1} \boldsymbol{\Sigma}_a \mathbf{u}_k = \gamma_k \mathbf{u}_k$ , where the  $\gamma_k$  are the ordered eigenvalues of  $\boldsymbol{\Sigma}_t^{-1} \boldsymbol{\Sigma}_a$  and the  $\mathbf{u}_k$  are the associated right eigenvectors. This is equivalent to maximizing  $\mathcal{R} = (\mathbf{u}^T \boldsymbol{\Sigma}_w \mathbf{u})^{-1} (\mathbf{u}^T \boldsymbol{\Sigma}_a \mathbf{u})$ . The canonical variates,  $\mathbf{c}_k$ , can be normalized such that  $\text{var}(\mathbf{c}_k) = \mathbf{u}_k^T \boldsymbol{\Sigma}_t \mathbf{u}_k = 1$ . The discriminating patterns are then defined as the regression coeffi-

cients,  $\mathbf{p}_k = (\mathbf{u}_k^T \boldsymbol{\Sigma}_t \mathbf{u}_k)^{-1} \boldsymbol{\Sigma}_t \mathbf{u}_k$  of the centered data,  $\mathbf{X}$ , onto the  $\mathbf{c}_k$ 's.

## Appendix B

### Truncation

Since the number of variables (grid points) exceeds the number of observations, the system to be analyzed is overdetermined and the LDA is ill-posed. Therefore, the analysis must be regularized (Schneider and Held 2001; Hansen 1998). The LDA is performed using a truncated principal-component representation of the dataset; keeping only the leading  $r$  modes. Figure 10a depicts the dependence of the variance ratio,  $\mathcal{R} = v_b/v_w$ , on the choice of the truncation parameter,  $r$ . This example is drawn from the 2D LDA analysis performed in section 5a. The between-group variance,  $v_b$ , and within-group variance,  $v_w$ , are also independently shown. We can see that as  $r$  increases, both  $\mathcal{R}$  and  $v_b$  increase while  $v_w$  decreases. As the number of degrees of freedom grow, the discriminant is able to capture more of the large-scale variance between the groups while simultaneously becoming more orthogonal to the within-group variability. However, relative importance of  $v_b$  and  $v_w$  to  $\mathcal{R}$  does not stay consistent. Initially as  $r$  grows,  $r \leq 5$ , the change in  $\mathcal{R}$  is caused by changes in both  $v_b$  and  $v_w$ . For  $5 < r < 8$ ,  $\mathcal{R}$  is relatively stable. For  $r \geq 8$ , increases in  $\mathcal{R}$  are caused almost entirely by decreases in  $v_w$ , which is not desirable. This can be seen more clearly in Figure 10b which depicts the ratio of  $\mathcal{R}$  for neighboring values of  $r$ :  $\Delta R_1(r) = R_1(r)/R_1(r-1)$ . Similar ratios for  $v_b$  and  $v_w$  are also shown.

If  $r$  is too small, the model is missing variability important to the discrimination of the groups. This can be seen in rapid growth of  $\mathcal{R}$  for  $r \leq 5$ . On the other hand, if  $r$  is too large, the model is overfitting the data. Since the number of observations in each group is small, choosing a large

$r$  gives the model enough degrees of freedom to find a pattern which is nearly orthogonal to the within-group variability. This rapid decrease in  $v_w$  and associated rapid increase in  $\mathcal{R}$  is most likely an artifact of the small sample size. For this example, choosing  $5 \leq r \leq 7$  seems appropriate; we used  $r = 5$  for this analysis in this study.

It is important to note that the qualitative nature of results is robust for all but the smallest values of  $r$ . It is only the quantitative results, such as the variance ratio and its statistical significance, which depend upon this choice.

## References

- Butchart, N., S. A. Clough, T. N. Palmer, and P. J. Trevelyan, 1982: Simulations of an observed stratospheric warming with quasigeostrophic refractive-index as a model diagnostic. *Quart. J. Roy. Meteor. Soc.*, **108**, 475–502.
- Coughlin, K. and K. K. Tung, 2004a: 11-year solar cycle in the stratosphere extracted by the empirical mode decomposition method. *Adv. Space Res.*, **34**, 323–329.
- 2004b: Eleven-year solar cycle signal throughout the lower atmosphere. *J. Geophys. Res.*, **109**, D21105, doi:10.1029/2004JD004873.
- Dunkerton, T. J., D. P. Delisi, and M. P. Baldwin, 1988: Distribution of major stratospheric warmings in relation to the quasi-biennial oscillation. *Geophys. Res. Lett.*, **15**, 136–139.
- Garcia, R. R., 1987: On the mean meridional circulation of the middle atmosphere. *J. Atmos. Sci.*, **44**, 3599–3609.

- Gleisner, H. and P. Thejll, 2003: Patterns of tropospheric response to solar variability. *Geophys. Res. Lett.*, **30**, 1711, doi:10.1029/2003GL017129.
- Gray, L. J., S. Crooks, C. Pascoe, S. Sparrow, and M. Palmer, 2004: Solar and QBO influences on the timing of stratospheric sudden warmings. *J. Atmos. Sci.*, **61**, 2777–2796.
- Haigh, J. D., 2003: The effects of solar variability on the earth's climate. *Philos. Trans. Roy. Soc. London*, **361**, 95–111.
- Hansen, P. C., 1998: *Rank-Deficient and Discrete Ill-Posed Problems: Numerical Aspects of Linear Inversion*. SIAM Monographs on Mathematical Modeling and Computation, Society for Industrial and Applied Mathematics, 247 pp.
- Holton, J. R. and H. C. Tan, 1980: The influence of the equatorial quasi-biennial oscillation on the global circulation at 50 mb. *J. Atmos. Sci.*, **37**, 2200–2208.
- Labitzke, K., 1987: Sunspots, the QBO, and the stratospheric temperature in the north polar-region. *Geophys. Res. Lett.*, **14**, 535–537.
- Labitzke, K. and H. van Loon, 1988: Associations between the 11-year solar-cycle, the QBO and the atmosphere. Part I: the troposphere and stratosphere in the northern hemisphere in winter. *J. Atmos. Terr. Phys.*, **50**, 197–206.
- Matsuno, T., 1971: Dynamical model of stratospheric sudden warming. *J. Atmos. Sci.*, **28**, 1479–1494.
- McIntyre, M. E., 1982: How well do we understand the dynamics of stratospheric warmings. *J. Meteor. Soc. Japan*, **60**, 37–65.

- Naito, Y. and I. Hirota, 1997: Interannual variability of the northern winter stratospheric circulation related to the QBO and the solar cycle. *J. Meteor. Soc. Japan*, **75**, 925–937.
- Ripley, B. D., 1996: *Pattern Recognition and Neural Networks*. Cambridge University Press, 403 pp.
- Schneider, T. and I. M. Held, 2001: Discriminants of twentieth-century changes in earth surface temperatures. *J. Climate*, **14**, 249–254.
- Smith, A. K., 1989: An investigation of resonant waves in a numerical-model of an observed sudden stratospheric warming. *J. Atmos. Sci.*, **46**, 3038–3054.
- Tung, K. K., 1979: Theory of stationary long waves. Part III: Quasi-normal modes in a singular waveguide. *Mon. Wea. Rev.*, **107**, 751–774.
- Tung, K. K. and R. S. Lindzen, 1979a: Theory of stationary long waves. Part I: Simple theory of blocking. *Mon. Wea. Rev.*, **107**, 714–734.
- 1979b: Theory of stationary long waves. Part II: Resonant rossby waves in the presence of realistic vertical shears. *Mon. Wea. Rev.*, **107**, 735–750.
- Wilks, D. S., 1995: *Statistical Methods in the Atmospheric Sciences*. International Geophysics Series, Academic Press, 467 pp.

# List of Figures

1	Results of a 4-group LDA for the Feb.-Mar. average of the difference between 10-50 hPa geopotential surfaces for 1959 to 2005. Grouping based on both the solar cycle and 30 hPa equatorial QBO indices. $\Delta z = 50$ m corresponds to $\Delta T \approx 1$ °C. (a) Mean state (b) Scatter plot of the 1 <sup>st</sup> two canonical variates: $C_1$ and $C_2$ . (c) 1 <sup>st</sup> discriminant pattern, $P_1(\mathbf{x})$ , (d) 1 <sup>st</sup> CV time series: $C_1(t)$ . . . . .	22
2	Sum of the mean from the 4-group LDA and two projections onto the 1 <sup>st</sup> discriminant pattern: $\mu(\mathbf{x}) + C_1(t^*) \cdot P_1(\mathbf{x})$ . (a) SCmin-wQBO case: $t^* = 1988$ . (b) SCmax-wQBO case: $t^* = 1978$ . . . . .	23
3	Results of a 2-group LDA for the Feb.-Mar. average of the difference between 10-50 hPa geopotential surfaces from 1959 to 2005. Grouping based on phase of solar cycle only. (a) Discriminant pattern, $P_1(\mathbf{x})$ , (b) CV time series, $C_1(t)$ , (c) Mean state (black line) plus group-mean projections onto $P_1(\mathbf{x})$ for SCmax (red, x) and SCmin (blue, o) groups. Shaded regions show $1\sigma$ projections for both groups. (d) Monte Carlo distribution of variance ratios showing percentile of observed variance ratio, $\mathcal{R}_1$ . . . . .	24
4	As Figure 3 except LDA based on phase of solar cycle during westerly QBO years only. (red, +) denotes the SCmax-wQBO group; (blue, o) denotes the SCmin-wQBO group. . . . .	25
5	As Figure 3, except LDA based on phase of solar cycle during easterly QBO years only. (black, x) denotes the SCmax-eQBO group; (green, *) denotes the SCmin-eQBO group. (a) as Figure 3c for eQBO years. (b) CV times series, $C_1(t)$ . . . . .	26

6	Results of a 2-group LDA for the Jan.-Mar. average of the difference between 10-50 hPa geopotential surfaces for 1959 to 2005. Grouping based on phase of 30 hPa equatorial QBO only. (a) Mean state (black line) plus group-mean projections onto $P_1(\mathbf{x})$ for wQBO (red, $\circ$ ) and eQBO (green, $*$ ) groups. Shaded regions show $1\sigma$ projections for both groups. (b) CV time series, $C_1(t)$ . . . . .	27
7	As Figure 6 except LDA based on QBO phase during solar cycle minimums only. (blue, $\circ$ ) denotes the SCmin-wQBO group; (green, $*$ ) denotes the SCmin-eQBO group. . . . .	28
8	As Figure 7 except using only data from 1959 to 1990. . . . .	29
9	As Figure 6 except LDA based on QBO phase during solar cycle maximums only. (red, $+$ ) denotes the SCmax-wQBO group; (black, $x$ ) denotes the SCmax-eQBO group. . . . .	30
10	(a) Dependence of the variance ratio, $\mathcal{R}$ , on the EOF truncation number, $r$ , for the 2-group LDA from Section 5a. Between-group variance, $v_b$ , and the inverse of the within-group variance, $v_w^{-1}$ , also shown. (b) Ratio of neighboring values for the variances shown above; <i>e.g.</i> , $\Delta\mathcal{R} = \mathcal{R}(r) / \mathcal{R}(r - 1)$ . . . . .	31

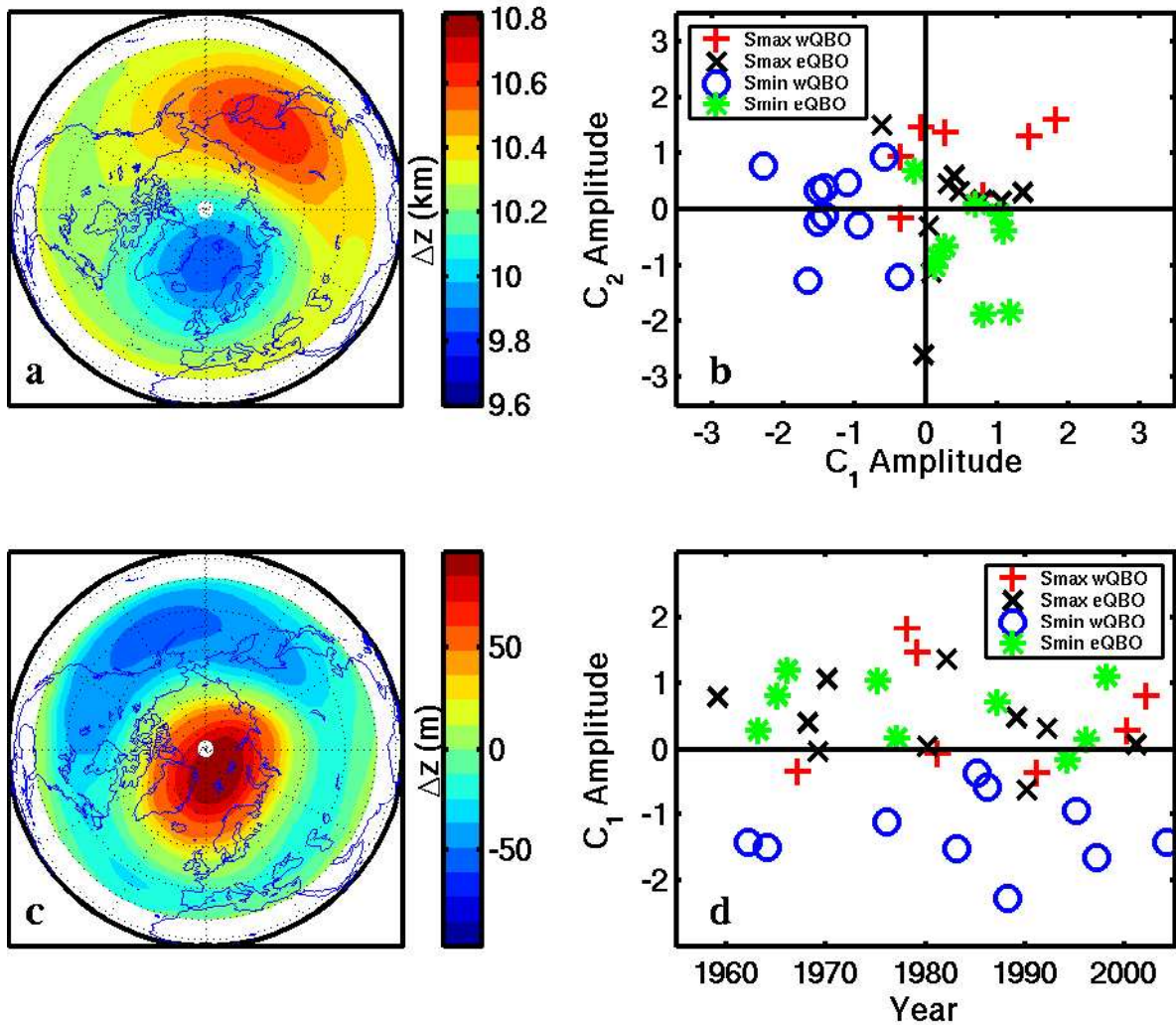


Figure 1: Results of a 4-group LDA for the Feb.-Mar. average of the difference between 10-50 hPa geopotential surfaces for 1959 to 2005. Grouping based on both the solar cycle and 30 hPa equatorial QBO indices.  $\Delta z = 50$  m corresponds to  $\Delta T \approx 1$  °C. (a) Mean state (b) Scatter plot of the 1<sup>st</sup> two canonical variates:  $C_1$  and  $C_2$ . (c) 1<sup>st</sup> discriminant pattern,  $P_1(x)$ , (d) 1<sup>st</sup> CV time series:  $C_1(t)$

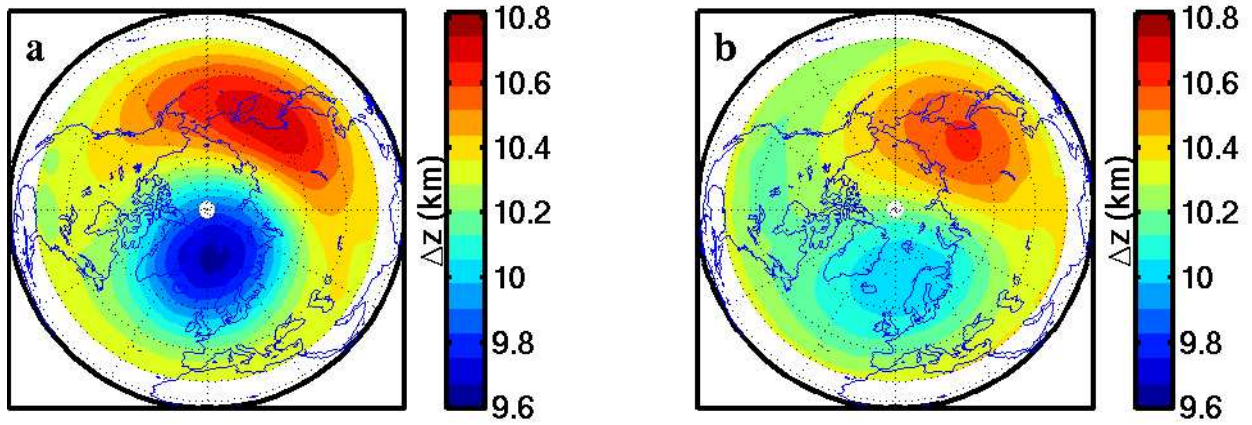


Figure 2: Sum of the mean from the 4-group LDA and two projections onto the 1<sup>st</sup> discriminant pattern:  $\mu(\mathbf{x}) + C_1(t^*) \cdot P_1(\mathbf{x})$ . (a) SCmin-wQBO case:  $t^* = 1988$ . (b) SCmax-wQBO case:  $t^* = 1978$ .

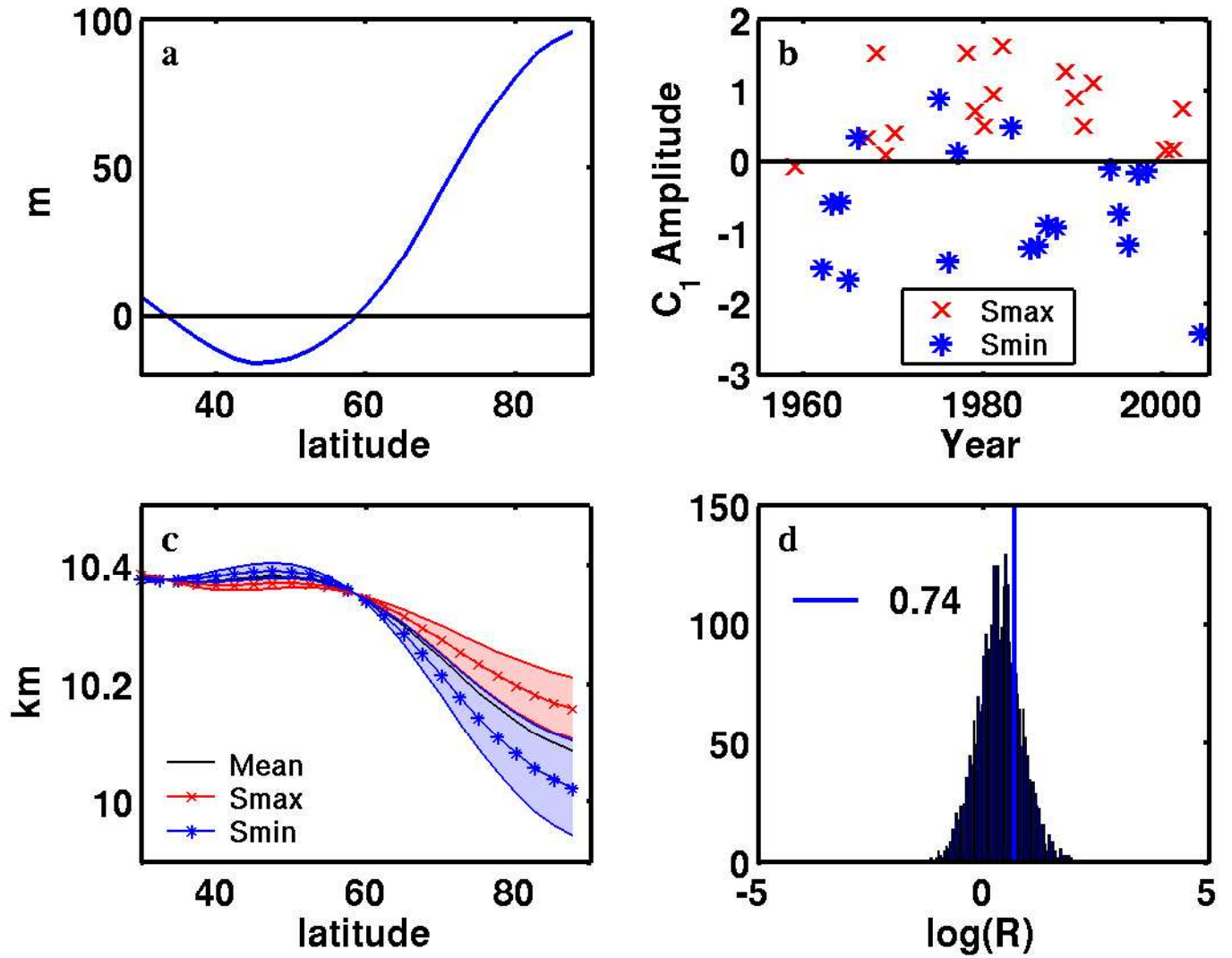


Figure 3: Results of a 2-group LDA for the Feb.-Mar. average of the difference between 10-50 hPa geopotential surfaces from 1959 to 2005. Grouping based on phase of solar cycle only. (a) Discriminant pattern,  $P_1(x)$ , (b) CV time series,  $C_1(t)$ , (c) Mean state (black line) plus group-mean projections onto  $P_1(x)$  for SCmax (red, x) and SCmin (blue, o) groups. Shaded regions show  $1\sigma$  projections for both groups. (d) Monte Carlo distribution of variance ratios showing percentile of observed variance ratio,  $\mathcal{R}_1$ .

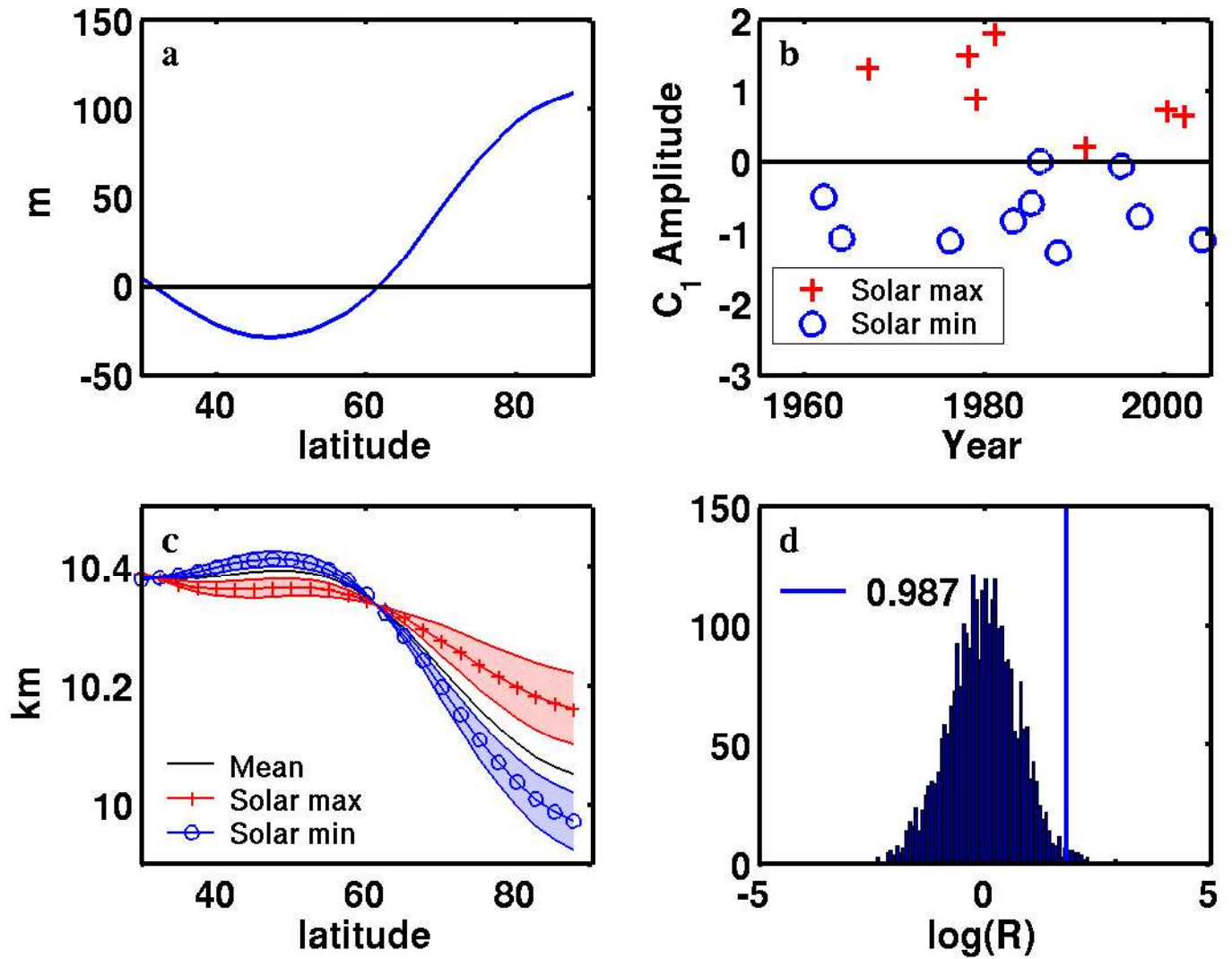


Figure 4: As Figure 3 except LDA based on phase of solar cycle during westerly QBO years only. (red, +) denotes the SCmax-wQBO group; (blue, o) denotes the SCmin-wQBO group.

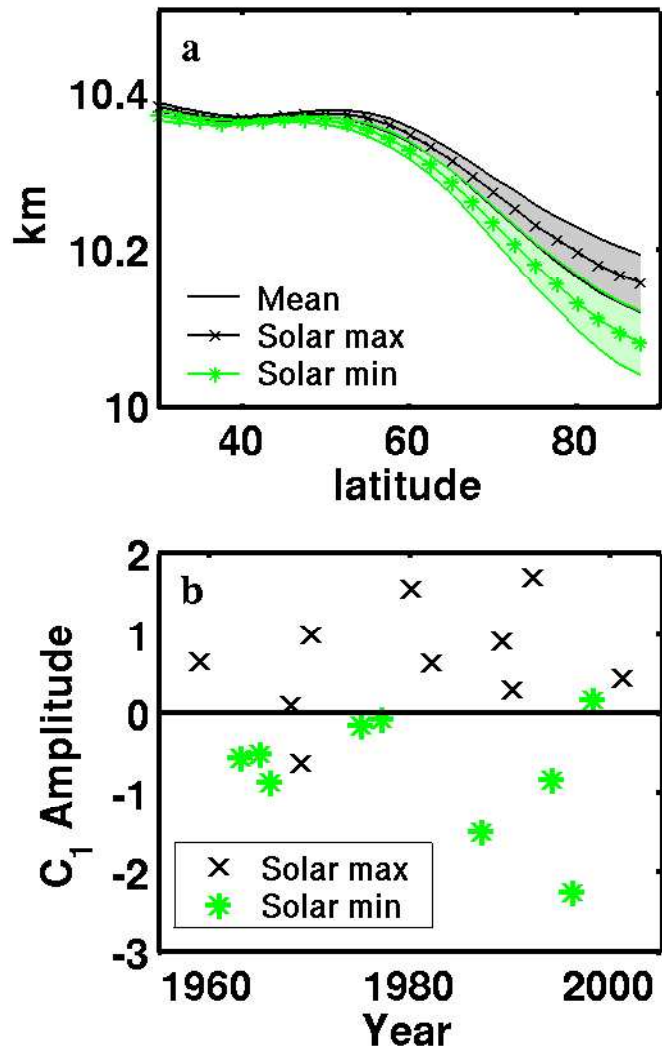


Figure 5: As Figure 3, except LDA based on phase of solar cycle during easterly QBO years only. (black, x) denotes the SCmax-eQBO group; (green, \*) denotes the SCmin-eQBO group. (a) as Figure 3c for eQBO years. (b) CV times series,  $C_1(t)$ .

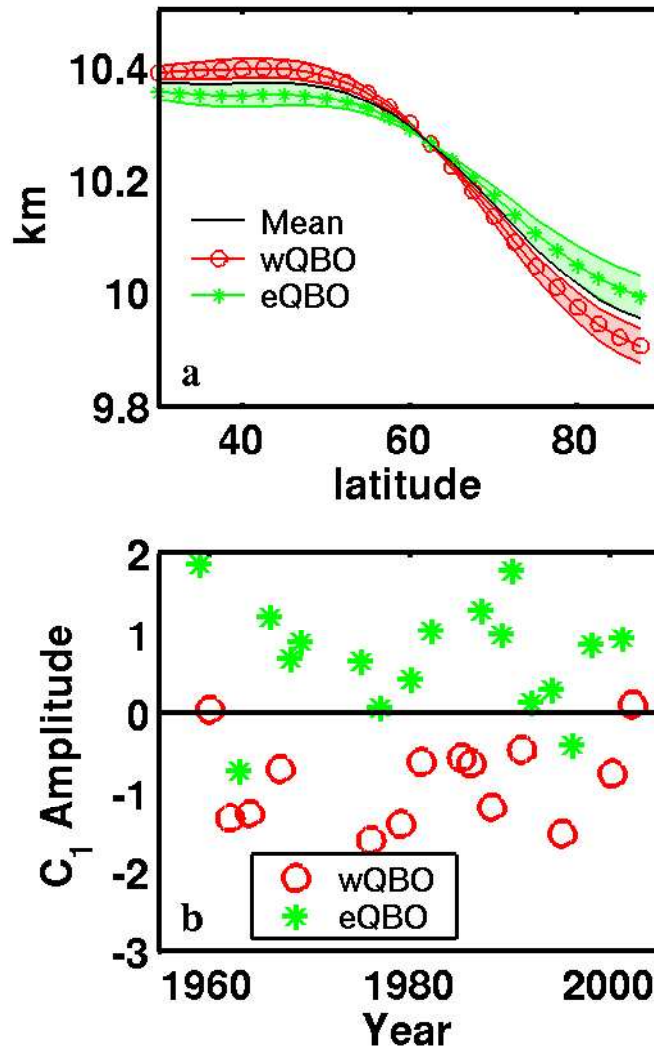


Figure 6: Results of a 2-group LDA for the Jan.-Mar. average of the difference between 10-50 hPa geopotential surfaces for 1959 to 2005. Grouping based on phase of 30 hPa equatorial QBO only. (a) Mean state (black line) plus group-mean projections onto  $P_1(x)$  for wQBO (red,  $\circ$ ) and eQBO (green,  $*$ ) groups. Shaded regions show  $1\sigma$  projections for both groups. (b) CV time series,  $C_1(t)$ .

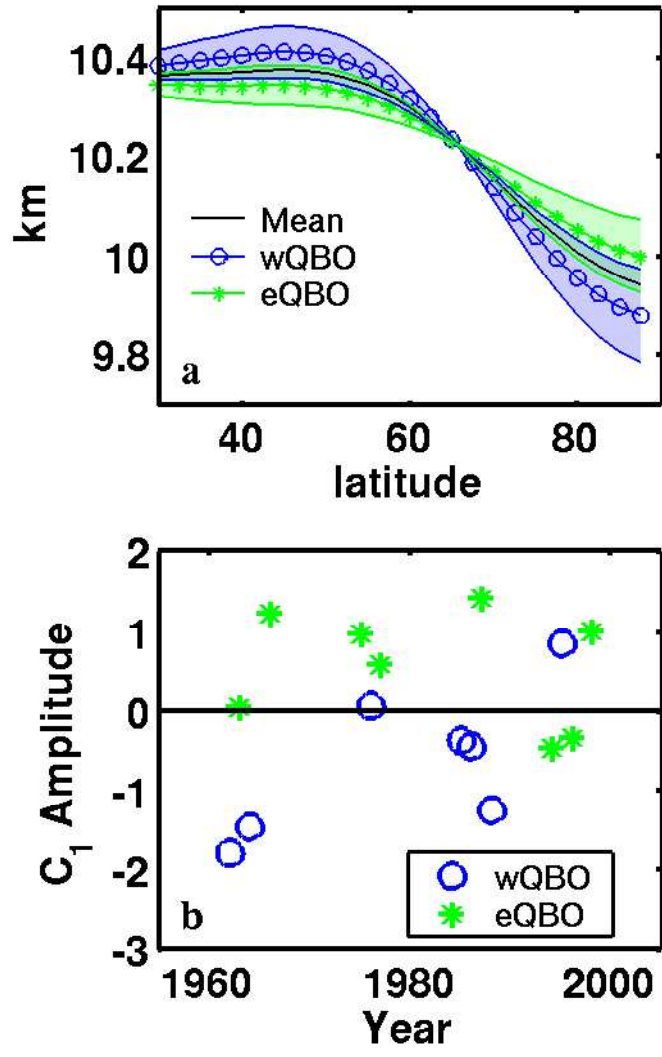


Figure 7: As Figure 6 except LDA based on QBO phase during solar cycle minimums only. (blue,  $\circ$ ) denotes the SCmin-wQBO group; (green,  $*$ ) denotes the SCmin-eQBO group.

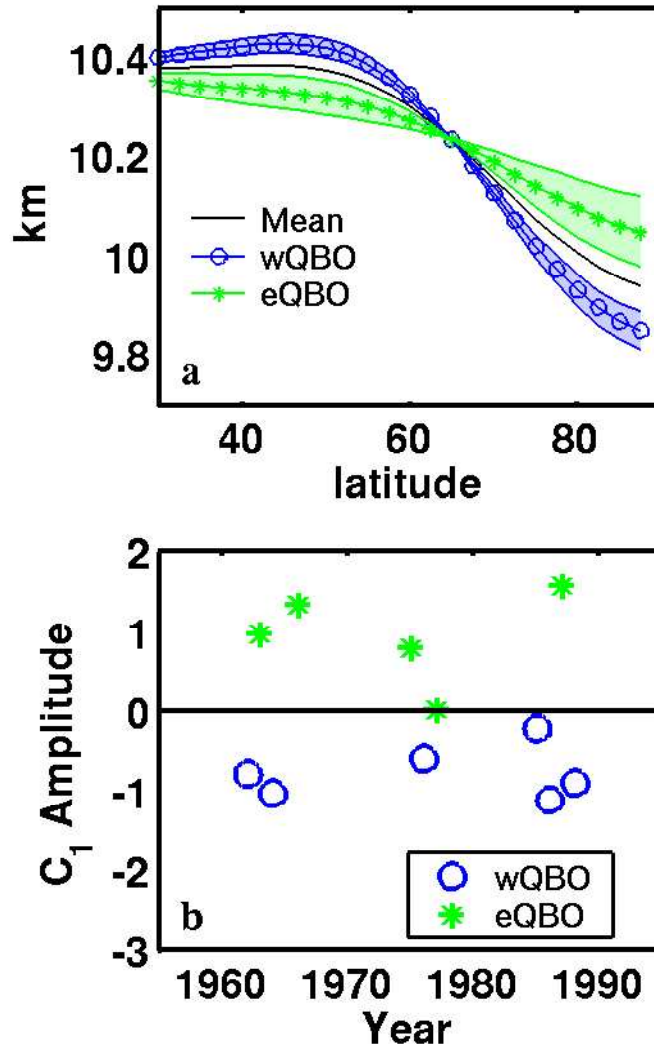


Figure 8: As Figure 7 except using only data from 1959 to 1990.

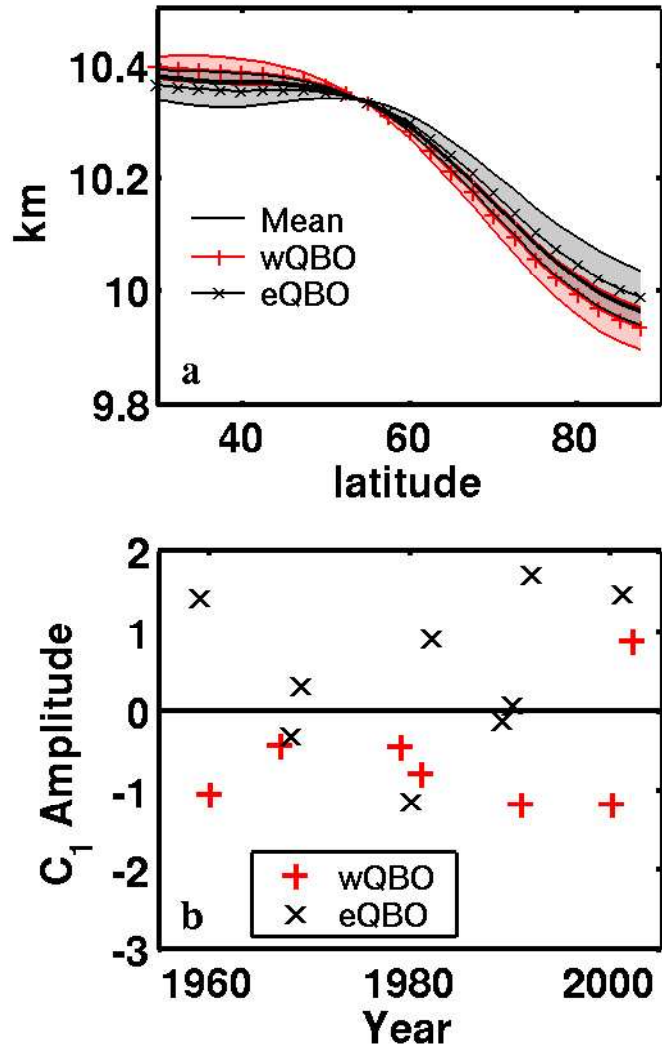


Figure 9: As Figure 6 except LDA based on QBO phase during solar cycle maximums only. (red, +) denotes the SCmax-wQBO group; (black, x) denotes the SCmax-eQBO group.

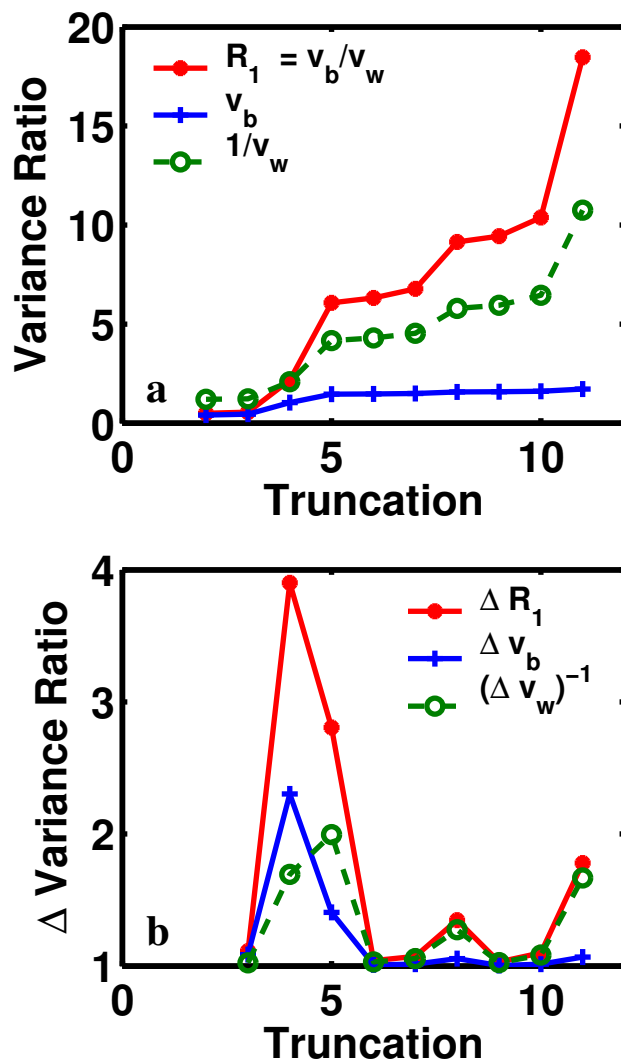


Figure 10: (a) Dependence of the variance ratio,  $\mathcal{R}$ , on the EOF truncation number,  $r$ , for the 2-group LDA from Section 5a. Between-group variance,  $v_b$ , and the inverse of the within-group variance,  $v_w^{-1}$ , also shown. (b) Ratio of neighboring values for the variances shown above; *e.g.*,  $\Delta\mathcal{R} = \mathcal{R}(r)/\mathcal{R}(r-1)$ .